



The influence of nonmigrating tides on the longitudinal variation of the equatorial electrojet

H. Lühr,¹ M. Rother,¹ K. Häusler,¹ P. Alken,² and S. Maus^{2,3}

Received 28 January 2008; revised 25 March 2008; accepted 25 April 2008; published 22 August 2008.

[1] The climatological model of the equatorial electrojet, EEJM-1, derived from Ørsted, CHAMP and SAC-C satellite measurements provides the opportunity to investigate the longitudinal variation of the current strength in detail. Special emphasis is put in this study on the effect of nonmigrating tides. We have found that the influence of the diurnal eastward-propagating mode with wavenumber-3, DE3, is particularly strong. In polar orbiting satellite observations the DE3 tidal signal appears as a four-peaked longitudinal structure. We have put special emphasis in our analysis to isolate the DE3 contribution from other sources contributing to the wavenumber-4 structure in satellite data. The amplitude of the DE3 signature in the EEJ not only peaks during equinox seasons, but is also strong around the June solstice. When looking at the modulation of the EEJ intensity the DE3 accounts for about 25% during the months of April through September. It is thus the dominant cause for longitudinal variations. During December solstice months the influence of DE3 is negligible. A secondary three-peaked longitudinal pattern emerges during solstice seasons when the DE3 influence is removed. From the data available it is, however, not clear whether this pattern is related to any tidal drivers.

Citation: Lühr, H., M. Rother, K. Häusler, P. Alken, and S. Maus (2008), The influence of nonmigrating tides on the longitudinal variation of the equatorial electrojet, *J. Geophys. Res.*, 113, A08313, doi:10.1029/2008JA013064.

1. Introduction

[2] The equatorial electrojet (EEJ) is a prominent current system on the dayside at dip-equator latitudes. This current has attracted significant attention since its discovery [e.g., Chapman, 1951; Forbush and Casaverde, 1961; Forbes, 1981; Onwumechili, 1997]. In spite of intensive research, one of the open issues has been the actual longitudinal variation of the EEJ intensity. From ground observations alone it is quite difficult to deduce the full longitudinal structure because of the fact that large parts of the dip-equator lie over the oceans. The first global picture of the EEJ was deduced from the POGO satellite observations [e.g., Onwumechili and Agu, 1981]. Later Langel *et al.* [1993] presented an EEJ profile from Magsat data. These latter observations were, however, limited to the 17–18 local time sector and the northern winter and spring seasons. The situation improved considerably after the launch of the three magnetic field mapping satellites, Ørsted, CHAMP and SAC-C, around the start of the new millennium. Longitudinal profiles derived from Ørsted observations have been presented by Jadhav *et al.* [2002] and Ivers *et al.* [2003]. Likewise, CHAMP data have been used by Lühr

et al. [2004] and Le Mouél *et al.* [2006]. There are some common features in all these curves, e.g., intensity peaks over South America and Indonesia, but otherwise they differ considerably. The situation has improved only recently. Alken and Maus [2007] performed a systematic study of the EEJ characteristics using all the data from the Ørsted, CHAMP and SAC-C satellites obtained during the years 1999–2006. On the basis of more than 95,000 EEJ samples they were able to construct a climatological model of the electrojet. From this model the longitudinal variations of the EEJ for various seasons, local times and solar flux intensities can be deduced.

[3] In a recent study England *et al.* [2006] pointed out that the noontime EEJ shows a four-peaked longitudinal structure during equinox seasons. The authors attributed this structure to a large-scale variation of the E-layer dynamo driven by tidal winds. It is increasingly evident that this kind of modulation is caused by nonmigrating tides originating in the tropical troposphere. For example, Forbes *et al.* [2006] analysed temperature measurements taken by the SABER instrument on board the TIMED satellite. They found an apparent wave-4 structure in longitude which is strong in the mesosphere, lower thermosphere (MLT) region. Similarly, Oberheide *et al.* [2006] reported a wave-4 structure in wind observations from TIDI on TIMED. The signature is most prominent in the zonal wind at MLT heights. From the eastward propagation of the wave fronts in a local time frame both groups concluded that this wave type can be related to the eastward propagating diurnal tide with zonal wavenumber-3 (DE3). This

¹GeoForschungsZentrum Potsdam, Potsdam, Germany.

²Cooperative Institute for Research in Environmental Sciences, University of Colorado, Boulder, Colorado, USA.

³National Geophysical Data Center, NOAA, Boulder, Colorado, USA.

statement is supported by results of the Global Scale Wave Model (GSWM) which predicts that the DE3 is primarily excited by latent heat release in the tropical troposphere and that this tidal mode is strong during large parts of the year [Hagan and Forbes, 2002]. Now also the seasonal variation of the DE3 signal in the MLT region has been observed. By analysing data from TIMED, Oberheide and Forbes [2008] found that this tidal component is strong in the temperature and zonal wind variations during the months April through November, with a maximum in August and minimum in February.

[4] Winds in the lower thermosphere drive currents through coupling with ions. We thus can expect an in-phase modulation of the ionospheric electric field with the tidal wave. Indeed, evidence of such a four-peaked longitudinal structure in the daytime ionospheric electric field has recently been presented. On the basis of vertical ion drift measurements Hartman and Heelis [2007] derived from DMSP data, taken at an altitude of 830 km and within the 9:30 local time (LT) sector, a wave-4 structure which peaks at the dip-equator during September. Independently, Kil *et al.* [2007] deduced similar results from ROCSAT-1 measurements at 600 km altitude.

[5] It is quite difficult to make systematic electric field measurements directly in the E-layer were the wind dynamo is most efficient during daytime. An indirect way of probing the electric field near dip-equator latitudes is measuring the intensity of the EEJ. The questions we want to address here: Which part of the EEJ signature (E-region electric field) can be attributed to DE3 tidal forcing? How does the DE3 influence changes with season?

[6] To answer these questions we make use of the predictions of EEJ peak current densities derived from the EEJM-1 climatological model of Alken and Maus [2007]. The interpretation will be based on the longitude versus local time distribution of the EEJ intensity.

[7] In the next section the properties of the DE3 signature will be introduced, and it is explained how this signature looks like in low-Earth orbiting (LEO) satellite observations. Subsequently, we describe our approach to distinguish the DE3 influence from other drivers of EEJ currents. The obtained results are discussed in the context of earlier studies of the DE3 tidal signal and other surveys of the EEJ longitudinal variation.

2. The DE3 Signature in Satellite Data

[8] In the recent literature an increasing number of publications report on four-peaked longitudinal structures in satellite observations. Often these signatures are related to a DE3 influence, but not always compelling evidence is provided for such a statement. Generally, a wave-4 signature in quasi sun-synchronous satellite data can be caused, for example, by a diurnal westward propagating DW5 tide, a stationary structure of wave-4, or a DE3 tide. However, the semidiurnal tide can also contribute to wave-4 with its components SW6 and SE2, as has been mentioned, e.g., by Forbes *et al.* [2006, equation (5)]. To distinguish between these different contributions one has to look into the phase change with local time. Figure 1 shows schematically the kinds of phase shifts expected for the three types of diurnal signals. For example, the DE3 wave fronts show an apparent eastward shift in satellite records by 90° within 24 hours

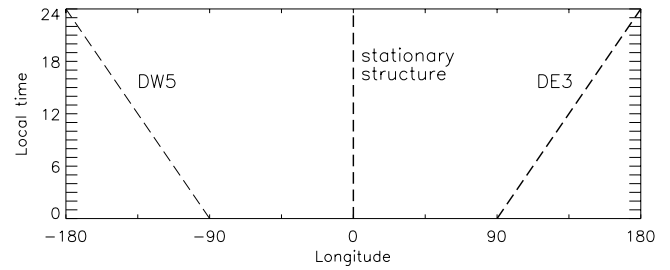


Figure 1. Ambiguity of wave-4 signature. A four-peaked longitudinal variation in satellite data can be caused by various sources: e.g., by the diurnal westward propagating tide, DW5 or eastward tide, DE3, or four-peaked stationary structure. They can be distinguished by their local time evolution.

in local time. When observed from ground they move eastward by 120° per day. It is the Doppler effect that causes the reduced speed in the satellite frame. Conversely, the DW5 is faster in the satellite frame, 90° westward per 24 hours compared to 72°, as seen from ground.

[9] The wave-4 signature observed by a LEO satellite, which moves slowly in local time, can be expressed for the diurnal terms as

$$A_4 \cos(4\lambda + \varphi) = a_3 \cos\left\{4\lambda - \frac{\pi}{12}(LT - t_3)\right\} + a_4 \cos\left\{4\lambda - \frac{\pi}{12}t_4\right\} + a_5 \cos\left\{4\lambda + \frac{\pi}{12}(LT - t_5)\right\}, \quad (1)$$

where A_4 is the amplitude of the total fourth harmonic, λ is the longitude, φ a local time-dependent phase shift, a_3 , a_4 , a_5 are the amplitudes of the signals driven by the different tidal components and t_3 , t_4 , t_5 are the times when the maxima of the tidal signals cross the 0°, 90°, 180° or 270° meridians. In cases where the signal is available from all longitudes and local times, equation (1) can be solved analytically for the six unknowns, a_3 , a_4 , a_5 and t_3 , t_4 , t_5 . Examples of such signals are the temperature and winds in the MLT [e.g., Forbes *et al.*, 2006; Oberheide *et al.*, 2006]. Such an analysis revealed the dominant role of DE3 in comparison to the other tidal components.

3. Determining the DE3 Signal in the EEJ

[10] The equatorial electrojet is a current system that is confined to the dayside. Primarily, this is due to the vanishing E-region conductivity during the dark hours. Therefore equation (1) cannot be solved directly. Instead we have used a numerical fitting procedure for quantifying the amplitudes and phases of the tidal modes.

[11] As an example of the diurnal EEJ evolution Figure 2 shows the peak current density distribution in a longitude versus local time frame for March equinox conditions. These values are derived from the EEJM-1 model of Alken and Maus [2007] for day of year (DoY) 80 and solar flux level, $F_{10.7} = 150$. It is quite evident that the current peaks around noon. Furthermore, there is a prominent four-peaked

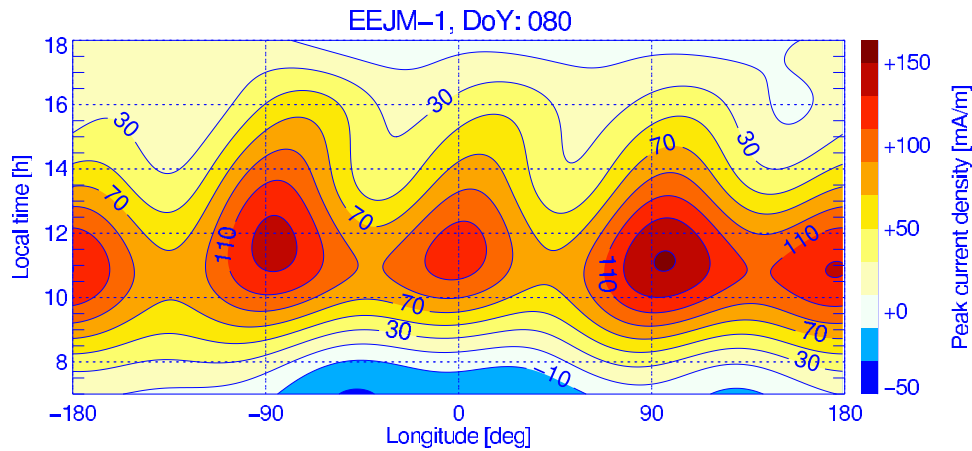


Figure 2. Longitudinal dependence of the diurnal variation of the EEJ peak current density at March equinox for solar flux, $F_{10.7} = 150$.

longitudinal variation. Subsequently, we will focus on interpreting this wave-4 structure.

[12] From the TIDI observations, for example, it is known that the intensity of the DE3-related signature in the winds at E-layer altitude varies little between day and night [Oberheide et al., 2006]. We therefore have to correct for the diurnal conductivity change before we can interpret the tidal signal properly. This is not a straightforward task because the diurnal variation of the EEJ intensity depends on the daily changes of both the electric field and the conductivity. Figure 3 shows the local time variation of the zonally averaged EEJ peak current density, as predicted by the EEJ model for a solar flux level of $F_{10.7} = 150$. There are separate curves for the days of the seasons (DoY: 80, 172, 264, 355). The two curves for the equinoxes are identical. This is due to the model parameterization which does not distinguish between Spring and Fall equinox, primarily to avoid model artifacts due to a lack of sufficient quiet-time passes during March equinox. During the equi-

nox seasons the EEJ is strongest and it peaks at 110 mA/m around 11 LT. The December curve is only 10% lower and peaks at about the same time. A significantly smaller amplitude (70 mA/m) is reached during the June solstice and the peak occurs later, at 12:20 LT.

[13] Since we are interested in the longitudinal variation of the electrojet, we have subtracted the zonal mean as a function of local time from each EEJM-1 sample point. This provides us with a data series that varies around zero. The next step is to find a suitable function for removing the effect of the changing E-layer conductivity. For this purpose we performed a few tests with the data set of DoY 80 (March equinox). As can be seen in Figure 2, the wave-4 pattern is rather dominant on that day. A spectral analysis of the detrended signal was performed over longitude for each local time hour. Then we checked the local time variation of the fourth harmonic since this is of prime interest here. Figure 4 shows, as a dotted curve, the relative diurnal variation of the wave-4 amplitude in EEJM-1. Peak ampli-

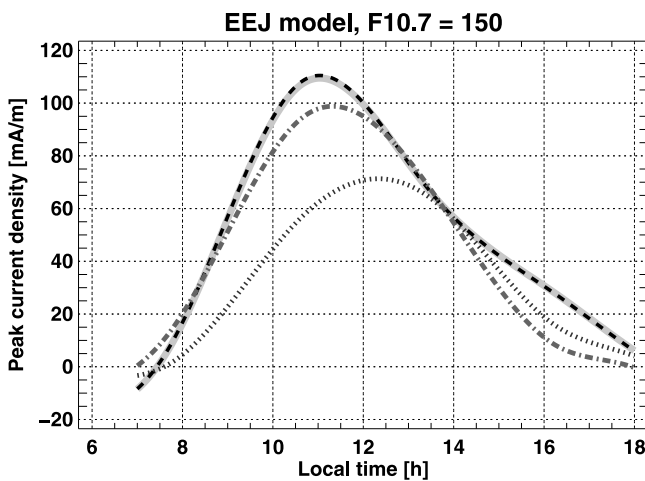


Figure 3. Zonal average of the EEJ local time variation. Diurnal variation of the peak current densities predicted by the EEJ model for the four seasons (March equinox, solid; June solstice, dotted; September equinox, dashed; December solstice, dashed-dotted).

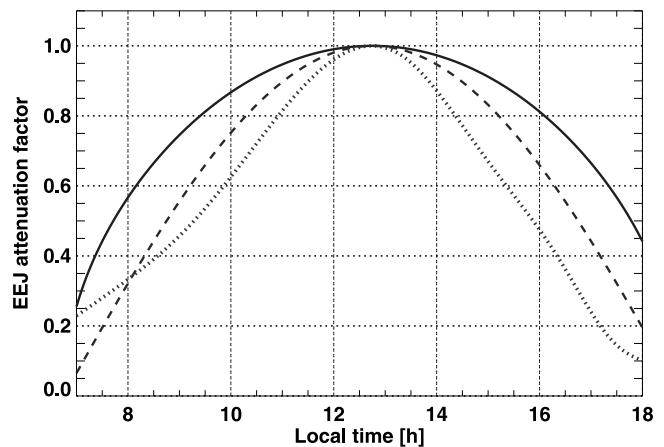


Figure 4. Different options for EEJ scaling functions. For the removal of the diurnal conductivity variation three functions have been tested: amplitude variation of the wave-4 signal in EEJM-1 (dotted), cosine of the local time (dashed) and square root of cosine (solid). All functions are centered at the time of the wave-4 peak amplitude (12:45 LT).

Table 1. Derived DE3 Tidal Signal (Amplitude, a_3 , and Phase, t_3) Derived From the EEJ Model for the Four Seasons

Day of Year	a_3 , mA/m	t_3 , UT	Degree of Modulation, %
80	23.5	11.4	21.4
172	17.0	9.4	24.3
264	22.9	11.4	20.8
355	5.7	0.6	5.7

tudes are reached at 12:45 LT. As alternatives we have also plotted curves of the cosine function (dashed line), $\cos(\frac{\pi}{12}(LT - t_0))$ and the square root of the cosine (full line), $[\cos(\frac{\pi}{12}(LT - t_0))]^{1/2}$. In all cases we used $t_0 = 12:45$. The question is which curve reproduces the diurnal conductivity variation best? For test purposes these three rescaling functions were applied to the bias-free signal of DoY 80 and then the DE3 signal was estimated using equation (1) (further details see below). Interestingly, the largest DE3 amplitude (a_3) was found when applying the square root of cosine rescaling. This is not obvious from Figure 4, but it is consistent with the expectation that the electron density of the E-layer varies proportional to the square root of the cosine of the solar zenith angle (as expected for an α -Chapman layer). The slight shift in time of the implied conductivity maximum may be explained by the delayed response of the ionosphere to the solar forcing. The square root of cosine function has subsequently been used for removing the conductivity effect in the EEJM-1 data of all seasons.

[14] For the actual determination of DE3 signatures in the EEJ intensity we made use of the detrended and rescaled model values of the days 80, 172, 264 and 355. Since the electrojet is active only over a part of the day, we had to estimate the DE3 amplitude and phase by fitting a function rather than by solving equation (1) analytically. The function (first term of equation (1))

$$F_{DE3} = a_3 \cos\left\{4\lambda - \frac{\pi}{12}(LT - t_3)\right\} \quad (2)$$

was fitted numerically to the array of model samples spanning all longitudes and the local times from 08 to 17 LT. This time sector is rather symmetrical with respect to the scaling function (cf. Figure 4). The parameters to be estimated are the amplitude, a_3 , and the phase, t_3 . As expected, large amplitudes of about 23 mA/m are found at equinox seasons. During June solstice the DE3 signature is somewhat smaller, and it is least pronounced in December. The peak of tidal signal crosses the Greenwich meridian shortly before noon at equinox and a little earlier in June, but it is out of phase in December. All derived values are listed in Table 1. Interestingly, the degree of longitudinal modulation of the EEJ by the DE3 tide, defined as the ratio of a_3 to peak diurnal amplitude (cf. Figure 3), is well above 20% during all seasons except for the December solstice, where it is reduced by about a factor of 4.

[15] Figure 5 summarizes the results of the DE3 tidal estimation. Here the spring equinox has not been shown since the EEJM-1 model does not resolve differences between the two equinox seasons. The top row displays the EEJ peak current density distribution, as derived from the EEJ model; in the middle we have the estimated DE3

signal, and at the bottom the remaining EEJ variations are shown after removing the DE3 tidal effects. These EEJ residuals are dominated by wave-2 longitudinal structures at equinox and by wave-3 features during solstices.

[16] In order to obtain a complete picture of the annual variation of the DE3 signature in the EEJ we have performed an analysis for every month of the year. Figure 6 shows the variations of the amplitude and phase (for definition see equation (1)). As expected, DE3 signatures are most pronounced around equinox, a little weaker in June, but largely reduced around the December solstice. The wave crest is passing the Greenwich meridian generally between 10 and 12 UT, except for December and January when the wave trough is passing this meridian shortly after 12 UT. We are not sure how reliable this latter phase switch is because of the small DE3 signal during December solstice season. In addition we show in Figure 6 the degree of longitudinal modulation of the EEJ caused by the DE3 tide. Here we obtain a somewhat different picture. Due to the reduced intensity of the EEJ around June solstice the relative modulation is constantly high in the middle of the year, varying around 25% from the beginning of April to the end of September. During the months around December solstice it is down to about 5%.

4. The Larger-Scale Longitudinal Structures

[17] In the previous section we found that larger-scale patterns dominate after removal of the DE3 tidal signal (cf. Figure 5, bottom row). Here we will have a closer look at these features. At equinoxes a double peak structure dominates. It is a well-known characteristic that the EEJ is strongest over South America and Indonesia [e.g., *Onwumechili*, 1997; *Lühr et al.*, 2004]. The situation is different during solstices. There we find three-peaked longitudinal structures. In order to further analyze this variation the approach described in the previous section is used again to proceed the investigation. Since we do not know which kind of tidal wave mode is responsible for the undulation, we fit a third harmonic function with constant phase at all local times to the residuals. For June solstice we obtain a constant phase wave-3 signal with an amplitude of 14.9 mA/m forming crests at -143° , -23° , and 97° longitude. For the December solstice we find a somewhat smaller wave-3 with amplitude 11.8 mA/m having crests at -173° , -53° , and 67° longitude. For test purposes we have repeated the analysis of the wave-3 signal without imposing any constrain. In that case we obtain for June Solstice 16 mA/m (+7%) and for December solstice 18 mA/m (+50%). This can be regarded as an indication that the constant phase assumption is less justified for December.

[18] Figure 7 shows the remaining EEJ residuals of the two solstice cases. For the June solstice we find two dominant patches, similar to the equinox cases appearing at -90° and 90° longitude. A secondary maximum shows up at a fairly late local time, 15 LT, around -140° long. The residuals for December solstice are markedly different. The electrojet intensity is rather constant around the globe with the exception of a marked minimum around 55° longitude. While we observed a late EEJ intensity peak in the eastern Pacific during June, a similar maximum is found at early local times in this longitude sector during December. After

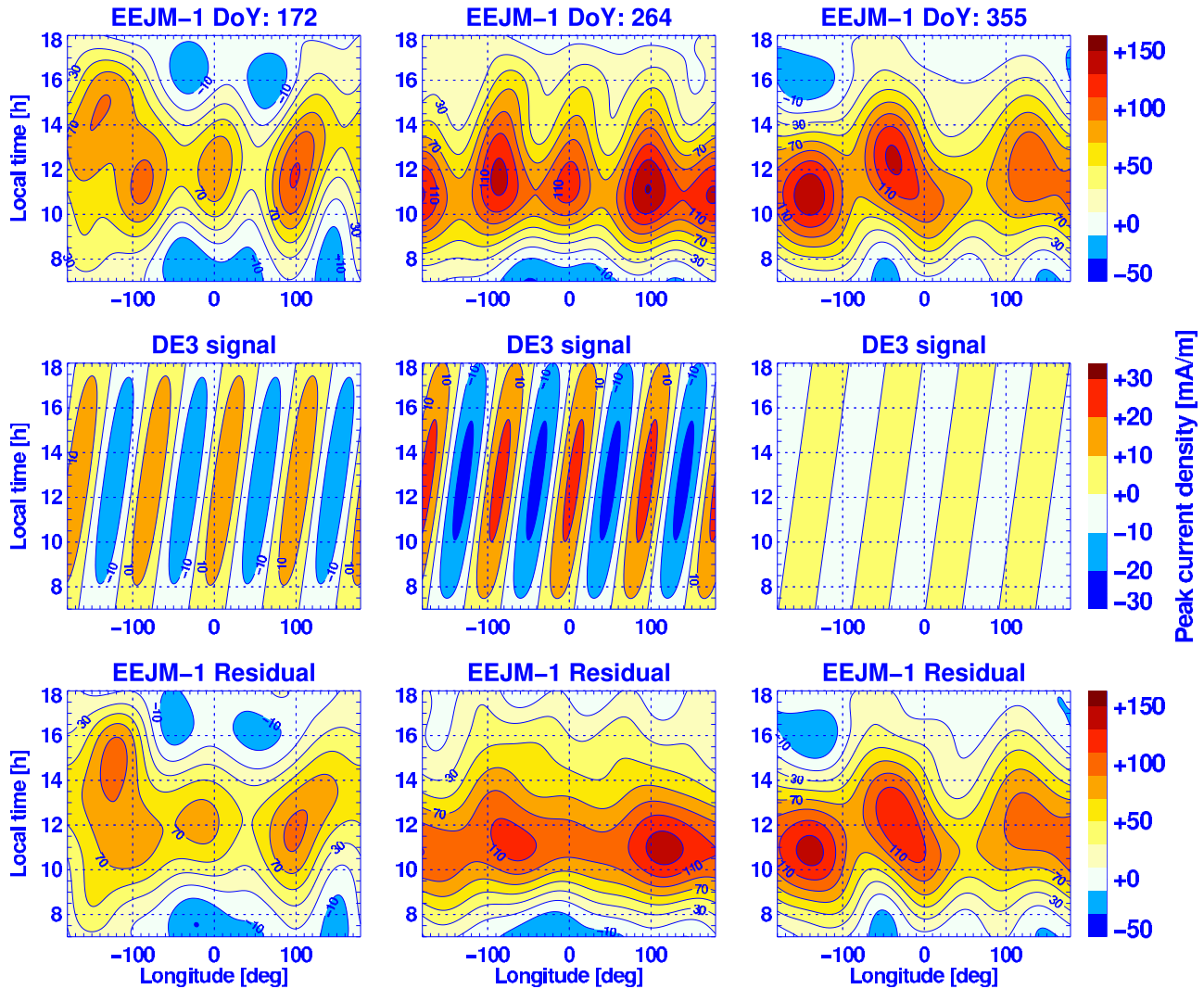


Figure 5. Determination of the DE3 tidal mode in the EEJ. The top row shows the longitudinal dependence of the EEJ diurnal variation for the different seasons as given by EEJ-M1. The middle row shows the extracted DE3 signals and the bottom row shows the remaining longitudinal variation.

removing prominent tidal influences obviously other differences between solstices become prominent in the remaining EEJ patterns.

5. Discussion

[19] In this study we have made use of the EEJ model presented by *Alken and Maus [2007]* for investigating the seasonal/longitudinal variations of the electrojet intensity. This model offers for the first time a global and comprehensive overview of the climatological features and the influence of nonmigrating tides on the current density. Since tidal forcing has not been used as a priori information when compiling the model, it is well suited for studying this aspect.

[20] Already *England et al. [2006]* had suggested that the tidal component DE3 is modulating the electrojet strength during March equinox. Here we have isolated this tidal component more rigorously by considering both its frequency and phase. As expected, we can confirm that the DE3 tide is an important mode for the electrojet modulation.

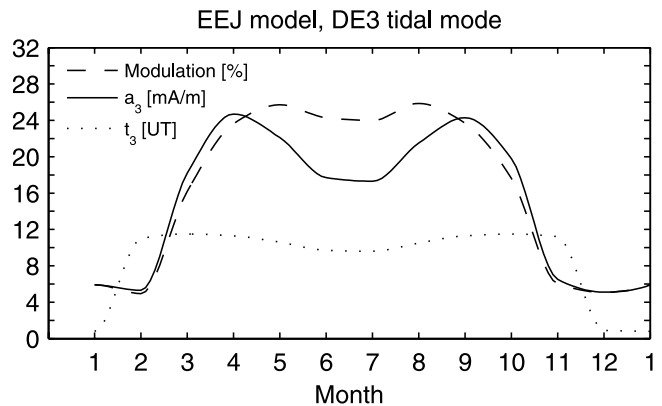


Figure 6. Annual variation of the DE3 tidal mode in the EEJ. The amplitude of the DE3 signal is shown as solid line, the phase of the signal is plotted as dotted line, and the relative modulation of the EEJ longitudinal variation is drawn as dashed line. The numbers at the abscissa mark the beginning of a month. Note that the similarity between the equinoxes may be due to the simplified model parameterization.

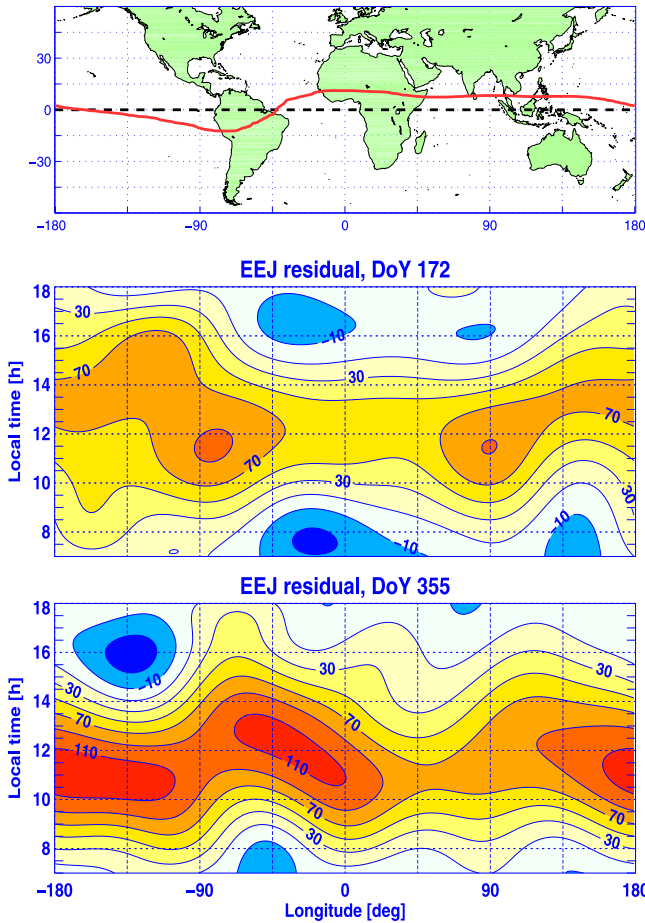


Figure 7. Secondary residuals of the EEJ current density after the removal of an additional wave-3 stationary structure. The longitudinal structures are quite smooth now. The local times of peak intensity tend to shift in opposite directions between June (top) and December solstice (bottom). For reference, a world map including the dip-equator is shown at the top.

It dominates the longitudinal variations during all seasons except for December solstice.

5.1. Estimation of E-Region Electric Field Variations

[21] The EEJ current density can be considered as a response to the zonal electric field, E_{zonal} , at E-layer altitude. *Alken and Maus* [2007] have tested this assumption by correlating the EEJ peak current density as derived from CHAMP magnetic field data with vertical drift measurements of the JULIA radar (Peru) at 150 km altitude. For obtaining a good linear correlation between current density, J_{peak} and plasma drift they had to introduce a function for the conductance, which depends on solar zenith angle and solar flux.

$$J_{peak} = \Sigma_C \cdot E_{zonal} \quad (3)$$

where Σ_C is the height-integrated, effective conductivity. For noontime and $F10.7 = 150$, which is used in this study, they obtain a value, $\Sigma_C = 291$ S. The plasma drift, v , is related to the electric field through the $\mathbf{E} \times \mathbf{B}$ relation.

When considering the magnetic field strength at 150 km above JULIA we obtain for the ratio v over E , 1 m/s over $24.4 \mu\text{V/m}$. Inserting this value into equation (3) reveals the relation between current density and vertical drift, valid over Peru, $J_{EEJ} = 7.1 v_z$, where J is measured in mA/m and v in m/s.

[22] For equinox we find a DE3-related variation of the EEJ current with an amplitude of 23 mA/m. This is equivalent to a vertical drift variation of 3.2 m/s over Peru (75°W). Such a small drift change is difficult to measure by satellite instruments. Although, so far no dedicated study has been performed identifying the DE3 signal in electric field variations, there are some reports on in situ detection of wave-4 signatures in vertical plasma drift. For example, *Hartman and Heelis* [2007] employed DMSP satellite data and identified wave-4 longitudinal structures above the dip-equator during the month September 2002. The amplitude of the wave amounts to about 6 m/s in the Peruvian sector at 830 km altitude. This is almost double the value we estimated. In another study, based on ROCSAT data from the years 1999.3 to 2004.5, *Kil et al.* [2007] also found a wave-4 signature in the prenoon vertical drift data. The amplitude, which is an average over all seasons, amounts to 2.1 m/s in the Peruvian sector at 600 km altitude. This much smaller value fits better our prediction when considering that the DE3 forcing is active for three quarters of a year (cf. Figure 6).

[23] Concerning the phase of the signal, *Hartman and Heelis* [2007] found peaks in vertical drift at longitudes of 0° and multiples of 90° in their measurements performed at 09:30 LT. Similarly, *Kil et al.* [2007] reported drift peaks on average 4° further east at 10:30 LT. These two observations are mutually consistent because the DE3 wave front propagates eastward by 3.75° per hour. From Table 1 we see that our analysis of the EEJ model reveals 11.4 UT as the time for the DE3 wave crest to pass the Greenwich meridian. This is about 2 hours later than the time derived from the plasma drift data. The difference can be explained by the fact that we have considered in our phase analysis only the DE3-related signal, while the compared plasma drift measurements contain the influences of all wave-4 drivers, not only DE3.

[24] In order to test this hypothesis we have analysed the total fourth harmonic signal of the EEJ variation from September equinox. Figure 8 shows the eastward shift of

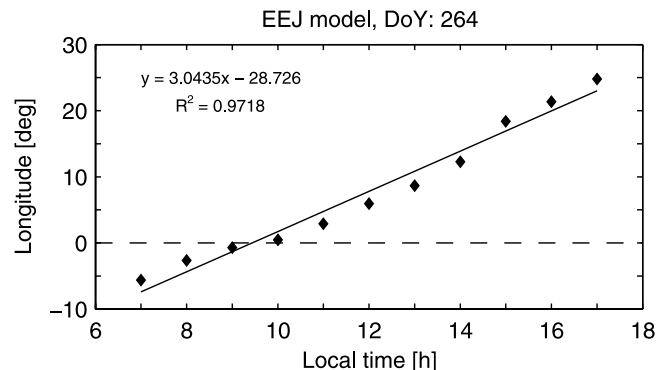


Figure 8. Shift in longitude of the EEJ total wave-4 crest versus local time. The equinox case is shown.

the wave-4 signal crest versus local time. We obtain a linear slope of 3.04° in longitude per local time hour. This is somewhat less than the 3.75° per hour of the DE3 signal and suggests the existence of other drivers, such as outlined on the right side in equation (1). The EEJ wave-4 crest crosses the Greenwich meridian at 9:30 LT, fully synchronously with the observed plasma drift variations. This good agreement provides additional confidence in the reliability of the EEJ model. The phase curve of Figure 8, valid for equinox conditions, should be considered in all direct comparisons of wave-4 signature in related quantities such as the electric field, vertical plasma drift, or EIA variations. It is interesting to note that the phase curve in Figure 8 shows a slight 12-hour period undulation. This may be caused by contributions of semidiurnal tidal components, SW6 and SE2, to the wave-4 signal. Zhang *et al.* [2006] reported significant wave power in these two tidal modes.

5.2. Longitudinal Variation other than Wave-4 Signals

[25] It is obvious from Figure 5 that the EEJ intensity exhibits significant longitudinal variations even after the removal of the contribution from DE3 tidal forcing. In case of equinox conditions we observe residual current density peaks at 120°E and at 75°W . These two longitude sectors are well-known for strong EEJs [e.g., Lühr *et al.*, 2004]. After removal of DE3 signatures wave-3 longitudinal structures become dominant during solstice seasons. We have applied another fit to the residuals using this time a function representing a stationary wave-3 signal. This choice is regarded to be arbitrary since we do not know the tidal mode that may be responsible for it. The revealed amplitudes of this wave type are comparable for both seasons (June 15 mA/m, Dec. 12 mA/m). This is in contrast to the DE3 influence, which is minimal during December solstice. When looking at the phase of the wave-3 signal we see that the maxima occur 30° further to the east during June solstice compared to December. It can be considered as a seasonal effect. After removing the wave-3 we obtain for the June solstice a double-peaked longitudinal variation with maxima at 90° east and west (cf. Figure 7), similar to the one from the equinox cases. Here we have another example of similarity between June solstice and equinoxes.

[26] In order to explain the remaining longitudinal variations of the EEJ one may look into electrodynamic model runs. For example, Dombia *et al.* [2007] used the Thermosphere-Ionosphere-Electrodynamics General Circulation Model (TIE-GCM) to simulate, among other effects, the longitudinal variation of the EEJ. For all seasons they found that the EEJ intensity peaks at 90°W and 130°E because of the deviation of the geomagnetic field from dipole geometry (see their figures 9 and 13). Although this is in reasonable agreement with our empirical model for the equinoxes and June solstice seasons, after removing the influences of nonmigrating tides, it fails to reproduce the December solstice observations appropriately.

[27] The December solstice seems to be different in several aspects. As can be seen in Figure 7, the remaining double-peaked structure is not comparable with the June and equinox cases. We may even ask ourselves whether it was justified and helpful to remove a wave-3 signal with fixed phase from the residuals in Figure 5. There we find maxima at about 50°W and 150°W . These EEJ intensity

peaks are close to the crossing points between dip-equator and geographic equator, at 43°W and 162°W longitudes. We may speculate that the interaction of the lower thermospheric winds with the plasma at the dip-equator causes enhanced zonal electric fields in the vicinity of these particular points. The fact that the separation of the crossover points is just 120° in longitude may have favored the apparent wave-3 pattern. Thus the identified stationary three-peaked longitudinal structure is possibly not related to any nonmigrating tidal wave. Further studies are needed to improve our understanding of the EEJ longitudinal variations around December solstice.

6. Conclusions

[28] We have analysed the longitudinal variation of the equatorial electrojet and its dependence on seasons. This study is based on the empirical EEJM-1 model of Alken and Maus [2007]. With this model it is possible for the first time to obtain a detailed picture of the EEJ behaviour on a global scale. We focus in the presented study on the influence of nonmigrating tides on the intensity of the EEJ. Such investigations can be performed effectively only from a global data set distributed evenly in space and time.

[29] Our major findings are:

[30] 1. The nonmigrating tidal mode DE3 has a strong impact on the EEJ intensity during three quarters of a year. During the months April to October it causes a modulation of the total current strength by 25%. Therefore DE3 is the largest contributor to the EEJ longitudinal variations. The influence of this nonmigrating tide is negligible during December solstice months.

[31] 2. During solstice months there appears in addition to DE3 a prominent wave-3 longitudinal pattern in EEJ intensity. This variation could not be linked to a tidal signal but is probably related to the crossing points between dip-equator and geographic equator.

[32] 3. Equinoxes and June solstice seasons show rather similar responses to tidal forcing. In both cases, after subtracting tidal contributions, the basic EEJ longitudinal variations exhibit intensity peaks over South America and Indonesia. These maxima in current strength can be explained by the deviation of the geomagnetic field from dipole geometry.

[33] 4. The results presented here may serve as a benchmark for testing the results of electrodynamic models such as TIE-GCM or CTIPE.

[34] While the EEJM-1 empirical electrojet model provides important new insight into the influence of nonmigrating tides on equatorial electrodynamics, two obstacles still stand in the way of a complete understanding. The first concerns the incomplete parameterization of the seasonal variation in EEJM-1, which does not capture possible differences between Spring and Fall equinox. With the continuously growing set of CHAMP observations at solar quiet conditions, it should be possible to refine the seasonal variation in the EEJM model by including further model parameters in the next model revision. A second uncertainty in the results presented here is introduced by the manner in which the diurnal change of the ionospheric conductivity is corrected for. Future studies should be devoted to improving this situation. Then the EEJ model of Alken and Maus

[2007] can also be used for characterizing the electric field in the E region.

[35] **Acknowledgments.** We thank J. Oberheide for fruitful discussions about nonmigrating tides. One of the authors (KH) is supported by the DFG Priority Program CAWSES, SPP1176.

[36] Amitava Bhattacharjee thanks Scott England and Arthur Richmond for their assistance in evaluating this paper.

References

- Alken, P., and S. Maus (2007), Spatio-temporal characterization of the equatorial electrojet from CHAMP, Ørsted, and SAC-C satellite measurements, *J. Geophys. Res.*, *112*, A09305, doi:10.1029/2007JA012524.
- Chapman, S. (1951), The equatorial electrojets detected from the abnormal electric currents distribution over Huancayo, Peru and elsewhere, *Arch. Meteorol. Geophys. Bioclimatol., Series A*, *4*, 368–390.
- Doumbia, V., A. Maute, and A. D. Richmond (2007), Simulation of equatorial electrojet magnetic effects with the thermosphere-ionosphere-electrodynamics general circulation model, *J. Geophys. Res.*, *112*, A09309, doi:10.1029/2007JA012308.
- England, S. L., S. Maus, T. L. Immel, and S. B. Mende (2006), Longitude variation of the E-region electric fields caused by atmospheric tides, *Geophys. Res. Lett.*, *33*, L21105, doi:10.1029/2006GL027465.
- Forbes, J. M. (1981), The equatorial electrojet, *Rev. Geophys. Space Phys.*, *19*, 469–504.
- Forbes, J. M., J. Russell, S. Miyahara, X. Zhang, S. Palo, M. Mlynczak, C. J. Mertens, and M. E. Hagan (2006), Troposphere-thermosphere tidal coupling as measured by the SABER instrument on TIMED during July-September 2002, *J. Geophys. Res.*, *111*, A10S06, doi:10.1029/2005JA011492.
- Forbush, S. E., and M. Casaverde (1961), *The Equatorial Electrojet in Peru*, Publ. 620, pp. 135, Carnegie. Inst., Washington, D. C.
- Hagan, M. E., and J. M. Forbes (2002), Migrating and nonmigrating diurnal tides in the middle and upper atmosphere excited by tropospheric latent heat release, *J. Geophys. Res.*, *107*(D24), 4754, doi:10.1029/2001JD001236.
- Hartman, W. A., and R. A. Heelis (2007), Longitudinal variations in the equatorial vertical drift in the topside ionosphere, *J. Geophys. Res.*, *112*, A03305, doi:10.1029/2006JA011773.
- Ivers, D., R. Stening, J. Turner, and D. Winch (2003), Equatorial electrojet from Ørsted scalar magnetic field observations, *J. Geophys. Res.*, *108*(A2), 1061, doi:10.1029/2002JA009310.
- Jadhav, G., M. Rajaram, and M. Rajaram (2002), A detailed study of equatorial electrojet phenomena using Ørsted satellite observations, *J. Geophys. Res.*, *107*(A8), 1175, doi:10.1029/2001JA000183.
- Kil, H., S.-J. Oh, M. C. Kelley, L. J. Paxton, S. L. England, E. Talaat, K.-W. Min, and S.-Y. Su (2007), Longitudinal structure of the vertical $\mathbf{E} \times \mathbf{B}$ drift and ion density seen from ROCSAT-1, *Geophys. Res. Lett.*, *34*, L14110, doi:10.1029/2007GL030018.
- Langel, R. A., M. Purucker, and M. Rajaram (1993), The equatorial electrojet and associated currents as seen in Magsat data, *J. Atmos. Terr. Phys.*, *55*, 1233–1269.
- Le Mouél, J.-P., P. Shebalin, and A. Chulliat (2006), The field of the equatorial electrojet from CHAMP data, *Ann. Geophys.*, *24*, 515–527.
- Lühr, H., S. Maus, and M. Rother (2004), The noon-time equatorial electrojet, its spatial features as determined by the CHAMP satellite, *J. Geophys. Res.*, *109*, A01306, doi:10.1029/2002JA009656.
- Oberheide, J., and J. M. Forbes (2008), Tidal propagation of deep tropical cloud signatures into the thermosphere from TIMED observations, *Geophys. Res. Lett.*, *35*, L04816, doi:10.1029/2007GL032397.
- Oberheide, J., Q. Wu, T. L. Killeen, M. E. Hagan, and R. G. Roble (2006), Diurnal nonmigrating tides from TIMED doppler interferometer wind data: Monthly climatologies and seasonal variations, *J. Geophys. Res.*, *111*, A10S03, doi:10.1029/2005JA011491.
- Onwumechili, C. A. (1997), *The Equatorial Electrojet*, Gordon and Breach, New York.
- Onwumechili, C. A., and C. E. Agu (1981), Longitudinal variation of equatorial electrojet parameters derived from POGO satellite observations, *Planet. Space Sci.*, *29*, 627–634.
- Zhang, X., J. M. Forbes, M. E. Hagan, J. M. Russell III, S. E. Palo, C. J. Mertens, and M. G. Mlynczak (2006), Monthly tidal temperatures 20–120 km from TIMED/SABER, *J. Geophys. Res.*, *111*, A10S08, doi:10.1029/2005JA011504.

P. Alken and S. Maus, National Geophysical Data Center, NOAA E/GC1, 325 Broadway, Boulder, CO 80305-3328, USA.

K. Häusler, H. Lühr, and M. Rother, GeoForschungsZentrum Potsdam, Telegrafenberg, D-14473 Potsdam, Germany. (hluehr@gfz-potsdam.de)